DBR, Sub-wavelength grating, and Photonic crystal slab Fabry-Perot cavity design using phase analysis by FDTD

Jae Hwan (Eric) Kim[1] and Lukas Chrostowski[1], Eric Bisaillon[2] and David V. Plant[2]

[1]*Electrical and Computer Engineering, University of British Columbia*
[2]*Electrical and Computer Engineering, McGill University*
erick@ece.ubc.ca lukasc@ece.ubc.ca

Abstract: We demonstrate a Finite-Difference Time-Domain (FDTD) phase methodology to estimate resonant wavelengths in Fabry-Perot (FP) cavity structures. We validate the phase method in a conventional Vertical-Cavity Surface-Emitting Laser (VCSEL) structure using a transfer-matrix method, and compare results with a FDTD reflectance method. We extend this approach to a Sub-Wavelength Grating (SWG) and a Photonic Crystal (Phc) slab, either of which may replace one of the Distributed Bragg Reflectors (DBRs) in the VCSEL, and predict resonant conditions with varying lithographic parameters. Finally, we compare the resonant tunabilities of three different VCSEL structures, taking quality factors into account.

OCIS codes: (230.5750) Resonators; (230.1480) Bragg Reflectors.

References and links

1. L. A. Coldren and S. W. Corzine, *Diode Lasers and Photonic Integrated Circuits*, (Wiley Interscience, 1995).
2. B. E. A. Saleh and M. C. Teich, *Fundamentals of Photonics*, (Wiley Interscience, 1991).
3. A. Yariv, *Optical Electronics in Modern Communications*, (Oxford University Press, 1997).
4. E. Bisaillon, D. Tan, B. Faraji, A. G. Kirk, L. Chrowstowski, and D. V. Plant, "High reflectivity air-bridge subwavelength grating reflector and Fabry-Perot cavity in AlGaAs/GaAs," Opt. Express. **14**, 2573-2582 (2006).
5. S. Boutami, B. B. Bakir, J.-L. Leclercq, X. Letartre, P. Rojo-Romeo, M. Garrigues, P. Viktorovitch, I. Sagnes, L. Legratiet, and M. Strassner, "Highly selective and compact tunable MOEMS photonic crystal Fabry-Perot filter," Opt. Express. **14**, 3129-3137 (2006).
6. M. C. Y. Huang, Y. Zhou and C. J. Chang-Hasnain, "A surface-emitting laser incorporating a high-index-contrast subwavelength grating," Nature Photon. **1**, 119-122 (2007).
7. C. J. Chang-Hasnain, "Tunable VCSEL," IEEE J. Sel. Top. Quantum Electron. **6**, 978-987 (2000).
8. S. Fan and J. D. Joannopoulos, "Analysis of guided resonances in photonic crystal slabs," Phys. Rev. B **65**, 235112 (2002).
9. W. Suh, M. F. Yanik, O. Solgaard, and S. Fana, "Displacement-sensitive photonic crystal structures based on guided resonance in photonic crystal slabs," Appl. Phys. Lett. **82**, 1999-2001 (2003).
10. O. Kilic, S. Kim, W. Suh, Y.-A. Peter, A. S. Sudbø, M. F. Yanik, S. Fan, and O. Solgaard, "Photonic Crystal slabs demonstrating strong broadband suppression of transmission in the presence of disorders," Opt. Lett. **29**, 2782-2784 (2004).

1. Introduction

A Fabry-Perot (FP) cavity, consisting of two partially transmitting parallel mirrors is a very useful device for filtering specific wavelengths or as a resonator structure for a laser cavity. There are several ways of predicting resonant wavelengths in a FP structure. First, we use the Transfer Matrix Method (TMM) [1]. This Technique is applicable to one-dimensional structures, such as Distributed Bragg Reflectors (DBRs). For higher dimensionality structures, more advanced techniques are necessary, such as Finite-Difference Time-Domain (FDTD). By using the FDTD method, we can obtain a reflectance (or transmittance) from the structure, then determine peaks in the reflectivity plot. However, this technique requires a substantial

#82702 - $15.00 USD Received 3 May 2007; revised 3 Jul 2007; accepted 9 Jul 2007; published 1 Aug 2007

time to run the simulation for accurate results. Also, one may have to run the simulations repeatedly to check the resonant wavelengths if any parameters affecting the resonance are changed (e.g., cavity length). In this regard, a phase analysis would be a good methodology for estimating resonant conditions and providing insight into the FP cavity design process, while reducing simulation time.

In a typical FP resonator, a phase shift imparted by a single roundtrip of the wave propagation is a multiple of 2π [2, 3]. For instance, a total phase response in Fig. 1(a) can be expressed as the summation of $\angle\phi_{mirror1}$, $\angle\phi_{cavity}$, $\angle\phi_{mirror2}$, and $\angle\phi_{cavity}$. In this simplified model, the easiest way to shift the resonant wavelength is to vary the cavity length, since this produces the phase shift of the cavity, which changes the resonant wavelength. Therefore, as long as the phase responses of components forming the FP cavity are well known, an exact prediction of resonances is possible in a simple but very effective way. In Fig. 1(b), a simplified conventional Vertical-Cavity Surface-Emitting Laser (VCSEL) structure consisting of a top and bottom DBR is shown. Here, the top and bottom DBR are represented as Mirror1 and Mirror2 in Fig. 1(a). VCSEL structures are analyzed in detail in the following sections.

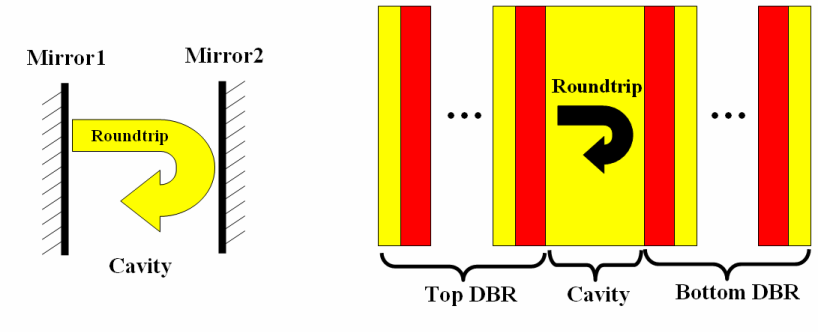

Fig. 1. (a). A simple diagram of a FP cavity assuming for normal incidence. Resonances occur when the roundtrip inside a cavity is a multiple of $2\pi m$ ($m = 0, \pm 1, \pm 2...$) and (b) a schematic diagram of a simple VCSEL structure forming a FP cavity.

In this paper, we use Lumerical FDTD software for FDTD phase and reflectivity calculations, and Matlab for TMM as well as resonant wavelength predictions based on phase. We start our phase analysis with DBRs and the conventional VCSEL structure, and estimate resonant wavelengths from the total phase response of the VCSEL, using both FDTD phase method and TMM. With the aim of proving our phase analysis to be valid, we compare our results with the FDTD reflectance method. Thereafter, we apply our phase analysis to highly reflective mirrors, such as a Sub-Wavelength Grating (SWG) and a Photonic Crystal (Phc) slab, and discuss how lithographic changes affect reflectivities and phases. We predict resonant conditions after the FP cavity is formed, while varying lithographically defined parameters. In the final section, we investigate maximum tuning ranges for VCSELs, including different types of highly reflective mirrors where corresponding quality factors (cavity Qs) are still above 1,000, by varying them either micromechanically (varying the cavity length) or lithographically (varying lithographic parameters).

2. VCSEL structure

The conventional VCSEL structure depicted in Fig. 1(b) is a good model for conducting a phase analysis. Here, we set a design wavelength for DBRs to 850nm, and choose the materials $Al_{0.12}Ga_{0.88}As$ (n=3.53) and $Al_{0.9}Ga_{0.1}As$ (n=3.03) to avoid any material absorption at the target wavelength. First, we choose 20 and 27 pairs of alternating $Al_{0.12}Ga_{0.88}As$ and

#82702 - $15.00 USD Received 3 May 2007; revised 3 Jul 2007; accepted 9 Jul 2007; published 1 Aug 2007

$Al_{0.9}Ga_{0.1}As$ for the top and bottom DBR mirrors, respectively which provide very high reflectivities (99.05% for 20 pairs and 99.9% for 27 pairs in FDTD simulations) at the 850nm wavelength.

For the phase analysis, we use FDTD simulations, where the phase of each DBR is determined by the electric fields being reflected from a single DBR after a TE polarized plane wave is incident to the structure (In this paper, we use the TE polarized plane wave for all the FDTD simulations). We vary the cavity length from 100nm to 190nm in 30nm increments, and compare changed resonances using both the FDTD phase and reflectance methods, to make sure that the phase analysis gives an exact prediction. In the phase plot, the resonance is determined at a point where the phase plot intersects at 0. As plotted in Fig. 2(a), the total phase moves up or down according to the cavity variation; as a result, the resonant wavelength becomes shorter (phase moving upward) or longer (phase moving downward). In Fig. 2(b), FP peaks in the stopband for various cavity lengths are shown. The shifting of those peaks is due to the phase shift demonstrated in Fig. 2(a), and shows a good agreement. For L=130nm, the resonant wavelength predicted by the FDTD phase and reflectance method is compared with TMM that shows a good agreement within 2nm.

In order to be able to accurately evaluate cavity Q values, the penetration depth of the DBR (l_{eff}) is considered in the calculation. l_{eff} can be calculated by finding 1) a 1/e point of the normalized electric field amplitude from the edge of the cavity to the DBR or 2) the mode spacing between resonant frequencies by increasing the cavity length to an integer number of λ. We use method 2) and increase the cavity length to 20λ, which reduces the mode spacing between resonant frequencies in the DBR stopband. The effective cavity length L_{eff} is written as $L_{eff} = L_{cavity} + l_{eff,topDBR} + l_{eff,bottomDBR}$. From the mode spacing (Δv) formula, penetration depths of both DBR pairs are then expressed as $l_{eff,topDBR} + l_{eff,bottomDBR} = \frac{c}{2n\Delta v} - L_{cavity}$ (where n = refractive index of the cavity and c = speed of light). Since we use same materials for the top and bottom DBR pairs, l_{eff} can be finally written as $l_{eff} = \frac{1}{2}(\frac{c}{2n\Delta v} - L_{cavity})$. According to our simulations, the penetration depth of the DBR is about 400nm. Therefore, for the VCSEL structure, we can write a formula for the Q calculation as $Q = v_0 \left[\frac{2\{nL_{cavity} + n_{eff,DBR}(l_{eff,topDBR} + l_{eff,bottomDBR})\}}{c} \right] Finesse$ (where v_0 =resonant frequency and $n_{eff,DBR}$ = refractive index of weighted average of DBR materials). Resonant wavelengths predicted by three different methods over different cavity lengths and corresponding quality factors (cavity Qs), calculated using the above formula, are summarized in Table 1.

#82702 - $15.00 USD Received 3 May 2007; revised 3 Jul 2007; accepted 9 Jul 2007; published 1 Aug 2007

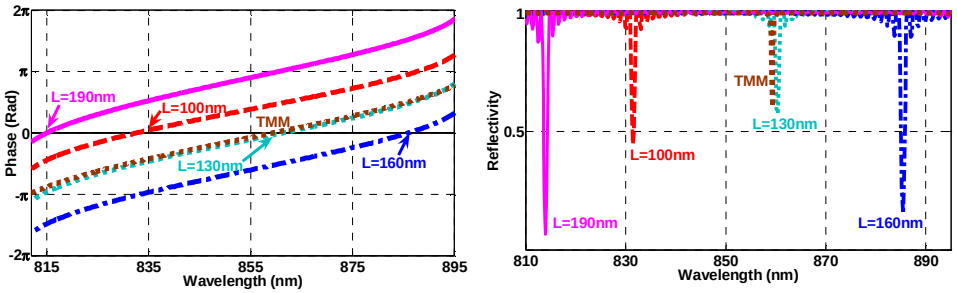

(a) (b)

Fig. 2. Resonant wavelengths of the VCSEL structure for various cavity lengths (L) estimated by (a) the phase analysis and (b) the notch reflectivity in the DBR stopband.

Table 1. Resonant Wavelengths Estimated by Three Different Methods, and Corresponding Cavity Qs.

Cavity Length (nm)	FDTD Reflectance Method (nm)	FDTD Phase Method (nm)	Transfer Matrix Method (nm)	Cavity Q Calculated
100	831.6	832.5	830.5	1,855
130	860.3	861.3	859.3	2,231
160	885.2	885.9	884.3	1,241
190	814.6	815.0	813.3	825

3. Periodic reflectors

We consider 1-D and 2-D periodic structures, namely a SWG and a Phc slab. High reflectivity can be exhibited from 0^{th} order wave-guide mode grating and the same phenomenon occurs for both structures.

Due to the feasibility of achieving high reflectivities, the SWG is considered to be a device that can replace one of the DBRs in a VCSEL or filter structures [4-6]. Reflectivity mostly depends on how the lithographically defined parameters, i.e., period (Λ) and duty factor (α) are set, as well as the thickness of the device. One of the most conspicuous advantages of using the SWG in the VCSEL is that it can vary the effective cavity length lithographically instead of by micromechanically tuning the cavity length, which requires an additional electrostatic force to be operated [7]. Also, by replacing a DBR a few micrometers thick (e.g., ~4um for 30 pairs intended for a 850nm wavelength) with a device that is hundreds of nanometers thick (e.g., ~250nm thick SWG or Phc slab in our design), it is possible to achieve a more compact-sized structure [4, 5].

Phc slabs provide unique characteristics in terms of supporting guided resonances whose electro-magnetic power is strongly confined within the slab, as well as in-plane guided modes that are completely confined by the slab without any coupling to external radiation [8]. A not very well-exploited property of Phc slabs is that a relatively wide range of high reflectivities is possible by appropriate settings of lithographic parameters such as the slab thickness, the square lattice constant (a) and the radius of the air hole (r) [8-10]. Similar to the SWG, Phc slabs are very useful for changing the effective cavity length lithographically rather than by micromechanical tuning.

#82702 - $15.00 USD Received 3 May 2007; revised 3 Jul 2007; accepted 9 Jul 2007; published 1 Aug 2007

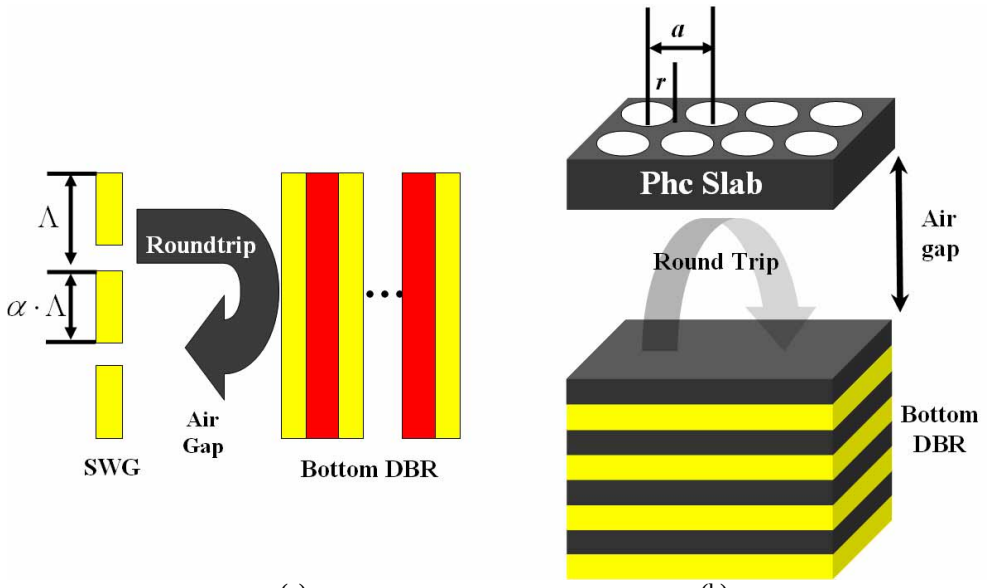

Fig. 3. The schematic diagram of two VCSEL structures, consisting of the air gap, 27.5 DBR pairs, and (a) the SWG and (b) the Phc slab forming the FP cavity.

3.1 Sub-wavelength grating

In this section, we examine the reflectivities and phases of a single SWG as a function of Λ and α and resonant conditions of the VCSEL, with the SWG used as a top mirror and 27.5 bottom DBR pairs. We choose $Al_{0.12}Ga_{0.88}As$ for the SWG slab and set design parameters to Λ = 420nm, $\alpha \cdot \Lambda$ = 310nm (α =0.738), and the thickness of the SWG to 163nm, so that high reflectivities are placed at the design wavelength. In Fig. 3(a), definitions of Λ and α in the SWG (assuming air-suspended), as well as a schematic diagram of the VCSEL incorporating the SWG, the cavity, and 27.5 DBR pairs are shown. As a consequence of using the 163nm thick SWG instead of 20 pairs of 2.6um thick DBR, the resonator is far smaller.
For the cavity design, we set the air gap to 860nm, in order that the resonant peak occurs at the target wavelength. The air gap plays an important role in providing a high refractive index contrast for the SWG. Sacrificial etch relaxes the etching tolerance and leaves a smooth surface in fabrication [4].

We determine the reflectivities and phases of a single SWG while varying the lithographic parameters. In Fig. 4, the duty factor (α) is first changed to 0.643, 0.690, and 0.738 (plots A, B, and C, respectively), while the period (Λ) is fixed at 420nm. Then, Λ is adjusted to 420nm, 440nm, and 460nm (plots C, D, and E, respectively), while α is set to 0.738. In other words, the plots A→ C and C→ E show effects of α and Λ on reflectivities and phases. With increasing α or Λ, not only do peak reflectivities tend to shift to longer wavelengths (Fig. 4(a)), but phases are apt to move in a downward direction (Fig. 4(b)). Based on these results, it is clear that varying the SWG lithographic parameters α or Λ can produce the phase shift.

#82702 - $15.00 USD Received 3 May 2007; revised 3 Jul 2007; accepted 9 Jul 2007; published 1 Aug 2007

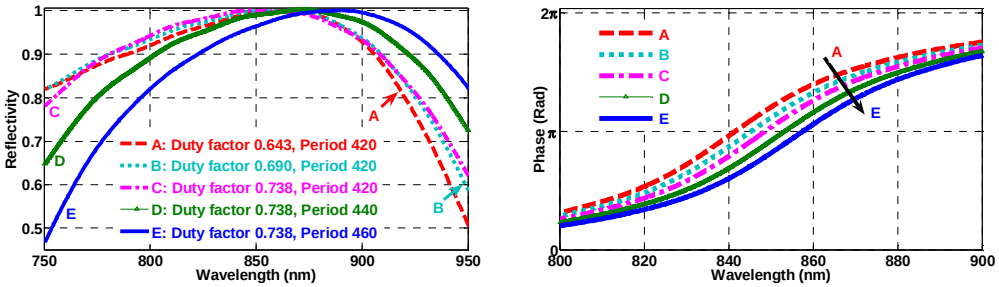

(a) (b)

Fig. 4. (a). Reflectivities and (b) phases of a single SWG as varying the duty factor (A→ C) and the period (C→E).

In Fig. 5(a), we determine phases of the SWG VCSEL shown in Fig. 3(a) and estimate resonant wavelengths from phase plots. The total phase response of the SWG VCSEL is the sum of an individual phase of the SWG, the cavity (air gap), and 27.5 DBR pairs. Resonances can be predicted by measuring specific points where phase plots intersect at 0. By increasing either α (A→ C) or Λ (C→ E), the phase plot tends to move in a downward direction, which results in a longer resonant wavelength. FP peaks in the stopband are shown in Fig. 5(b), and are in a good agreement with the resonances shown in Fig. 5(a). Table 2 summarizes resonant wavelengths estimated by the FDTD phase and reflectance methods, and corresponding cavity Qs, using the formula introduced in the previous section. l_{eff} is determined with the same method used for the conventional VCSEL case. According to our FDTD simulations, the penetration depth of the SWG is about 386nm. The maximum discrepancy between the two methods is less than 1nm.

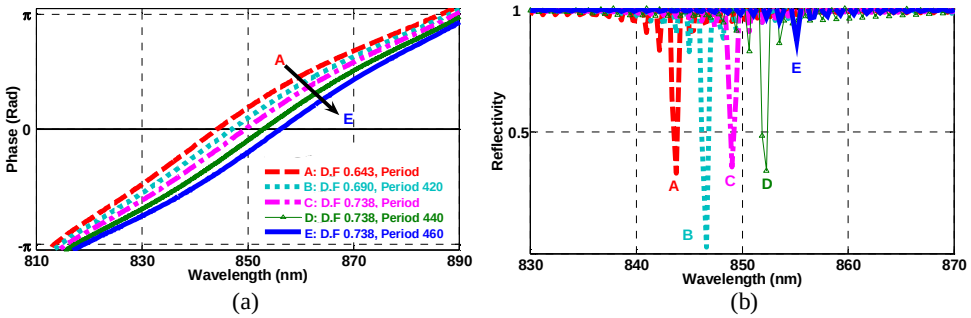

(a) (b)

Fig. 5. (a). Phase responses of the SWG VCSEL and (b) resonant wavelengths shown in the DBR stopband as the duty factor (A→ C) and the period (C→ E) are varied.

Table 2. Resonant Wavelengths Estimated by Two Different Methods, and Corresponding Cavity Qs.

Plot	α	Λ	FDTD Phase Method (nm)	FDTD Reflectance Method (nm)	Cavity Q Calculated
A	0.643	420	844.2	843.8	2,247
B	0.690	420	847.0	846.5	4,703
C	0.738	420	849.5	849.0	17,057
D	0.738	440	852.9	852.2	2,521
E	0.738	460	856.1	855.1	904

#82702 - $15.00 USD Received 3 May 2007; revised 3 Jul 2007; accepted 9 Jul 2007; published 1 Aug 2007

3.2. Photonic crystal slab

We select the $Al_{0.12}Ga_{0.88}As$ for the Phc slab material and set the slab thickness, the square lattice constant, and the radius of the air hole to 230nm, 446nm, and 0.48*a*, respectively, so that high reflectivities lie on the design wavelength.

In Fig. 3(b), definitions of *a* and *r* in a square lattice Phc slab, as well as a schematic diagram of the VCSEL incorporating the Phc slab as a top mirror, the cavity, and 27.5 bottom DBR pairs, are shown. For the cavity design, we set the air gap to 800nm, so that the resonant peak occurs at the design wavelength. The 800nm thick air gap and 27.5 bottom DBR pairs are used for the same reasons they were in the SWG VCSEL, described earlier.

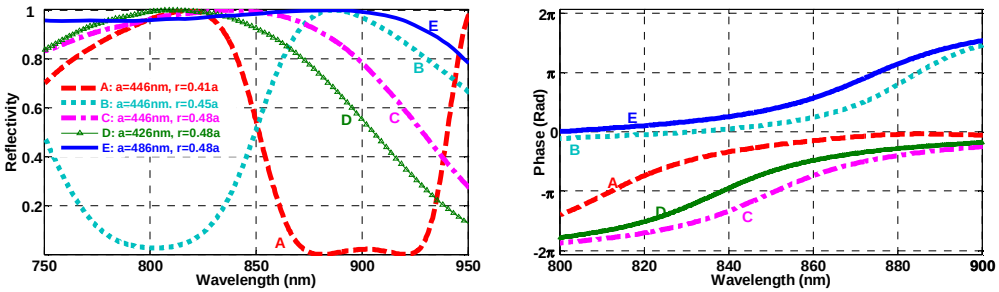

(a) (b)

Fig. 6. (a). Reflectivities and (b) phases of a single Phc slab as the radius of the air hole is adjusted (A→ B→ C), and the lattice constant is varied (D→ C→ E).

We determine reflectivities and phases of a single Phc slab under varying lithographic parameters. In Fig. 6, the radius of the air hole (*r*) is first changed to 0.41*a*, 0.45*a*, and 0.48*a* (plots A, B, and C, respectively), while the lattice constant (*a*) is fixed at 446nm. Then, *a* is changed to 446nm, 426nm, and 486nm (plots C, D, and E, respectively), while *r* is set to 0.48*a*. In Fig. 6(a), two high reflectivity peaks of plot A at around 820nm and 950nm are conspicuous, and tend to move to shorter wavelengths with increasing *r*. In other words, the high reflectivity peaks of plots B (at 880nm) and C (at 850nm) originate with the second highest peak of plot A. It is interesting that as *r* is increased, the high reflectivity span becomes broader. As well, as *a* is increased, not only do the high reflectivity peaks tend to shift to longer wavelengths (D→ C→ E), but also the high reflectivity span becomes wider. Very large air holes are more useful in terms of obtaining high reflectivities in a relatively wider wavelength range than are smaller holes due to the decreased lifetimes of guided resonances [9,10], but care should be taken in fabrication since adjacent holes are more likely to be connected with each other during e-beam lithography. In Fig. 6(b), the phase response of the Phc slab reflects the changes in lithographic parameters, with either *a* or *r* giving rise to the phase shift.

In Fig. 7(a), the phases of the Phc VCSEL (shown in Fig. 3(b)) over the stopband are plotted. Resonances can be predicted by measuring the intersections between each phase and the -2π, 0, and 2π coordinates. The effect of increasing *r* to 0.41*a*, 0.45*a*, and 0.48*a* (A→ B→ C, respectively) is to shift the phase plot upward (plot C appears below plot B due to a -2π phase shift). Also, increasing *a* to 426nm, 446nm, and 486nm (D→ C→ E, respectively), shifts the phase plot downward (plot E is shown above plot D owing to a 2π phase shift).

FP peaks in the stopband are shown in Fig. 7(b), and the results are in a good agreement with the phase analysis. Table 3 summarizes the resonant wavelengths estimated by FDTD

#82702 - $15.00 USD Received 3 May 2007; revised 3 Jul 2007; accepted 9 Jul 2007; published 1 Aug 2007

phase and reflectance methods and the corresponding cavity Qs. According to our FDTD simulations, the penetration depth of the Phc slab is about 949nm. The maximum discrepancy between the two methods is less than 1.5nm.

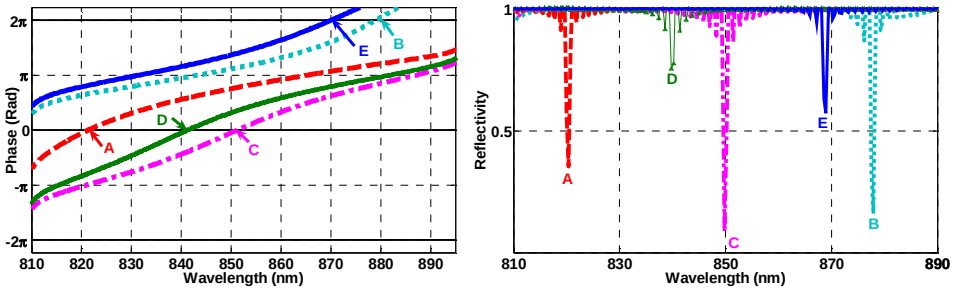

Fig. 7. (a). Phase responses of the Phc VCSEL and (b) resonant wavelengths shown in the stopband under varying *r* (A→ B→ C) and *a* (D→ C→ E).

Table 3. Resonant Wavelengths Estimated by Two Different Methods, and Corresponding Cavity Qs

Plot	***a***	***r***	**FDTD Phase Method (nm)**	**FDTD Reflectance Method (nm)**	**Cavity Q Calculated**
A	446	0.41*a*	821.4	820.4	12,090
B	446	0.45*a*	879.1	877.9	1,397
C	446	0.48*a*	851.2	849.8	4,354
D	426	0.48*a*	841.3	840.0	778
E	486	0.48*a*	870.1	868.9	6,225

4. Resonance tunability

In this section, we study maximum tunability and the corresponding cavity Qs for the three different VCSEL structures demonstrated previously. Resonance tuning is done by varying either the cavity or lithographic parameters; here, both methods are considered. Since we assume that cavity tuning is performed by varying the air gap between two mirrors, the air gap and is considered as the cavity for the conventional VCSEL structure shown in Fig. 1(b). Detailed design factors are summarized in Table 4.

Table 4. Three different VCSEL structures aimed at the 850nm resonant wavelength

Plot	**Structure**	**Mirror 1**	**Mirror 2**	**Cavity**
A	Conventional VCSEL	20.5 DBR pairs	27.5 DBR pairs	423nm air gap
B	SWG VCSEL	163nm thick SWG (α =0.738, Λ =420nm)		860nm air gap
C	Phc VCSEL	230nm thick Phc slab (*a*=446nm, *r*=0.48a)		800nm air gap

#82702 - $15.00 USD Received 3 May 2007; revised 3 Jul 2007; accepted 9 Jul 2007; published 1 Aug 2007

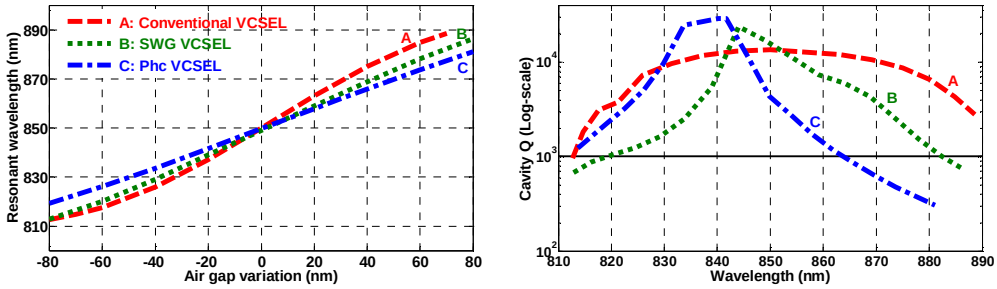

(a) (b)

Fig. 8. (a. Tuning slopes of the three different VCSEL structures according to air gap variation in the cavity and (b) corresponding cavity Qs at resonances.

First, we adjust the air gap from the designed cavity (air gap variation=0) for each structure in order to demonstrate their respective tuning sensitivities as shown in Fig. 8(a). The conventional VCSEL has the steepest tuning slope, representing the best micromechanical tunabililty, followed by the SWG VCSEL and the Phc VCSEL. In Fig. 8(b), the cavity Qs at resonances and maximum tunable ranges where Q values are higher than 1,000 are shown. The conventional VCSEL has the widest tunable range due to the high reflectivity plateau over the stopband, whereas the SWG VCSEL and Phc VCSEL provide limited ranges of high reflectivity of 61nm (820nm~881nm) and 48nm (815nm~863nm), respectively, as shown in Fig. 4(a) and Fig. 6(a).

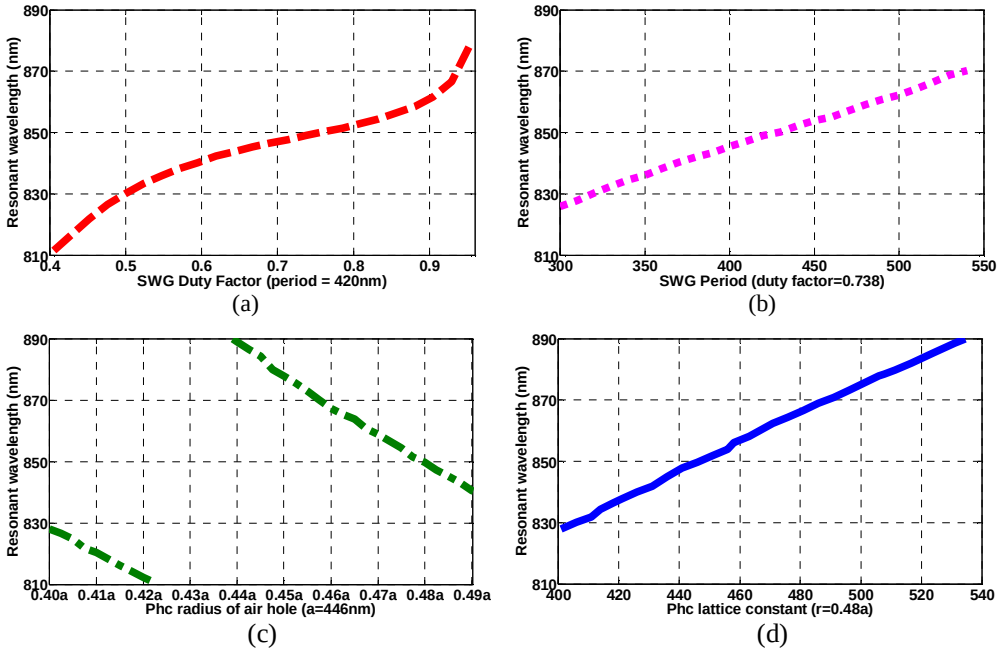

(a) (b) (c) (d)

Fig. 9. Resonance tuning by (a) SWG duty factor (α), (b) SWG period (Λ), (c) Phc radius of the air hole (r) and (d) Phc lattice constant (a).

Finally, we demonstrate resonance tuning by varying lithographic parameters for the SWG and Phc VCSELs in Figs. 9(a) - 9(d), and the maximum tunable ranges (Q >1,000) lithographically achievable in Fig. 10. The results show that the tunable ranges achieved by

#82702 - $15.00 USD Received 3 May 2007; revised 3 Jul 2007; accepted 9 Jul 2007; published 1 Aug 2007

varying α (SWG) and r (Phc slab) are approximately 60nm (817nm~877nm) and 61nm (813nm~824nm and 830nm~880nm), respectively. As well, resonance tuning by Λ (SWG) and a (Phc slab) is only possible in a relatively limited range for each, 14nm (SWG VCSEL) and 49nm (Phc VCSEL), respectively, which suggests that α and r are more effective than Λ and a for lithographic resonance tuning in VCSEL structures.

It is also interesting to note that for both SWG and Phc designs, there are two parameters that can be varied: this allows one to change both parameters to fine tune both the resonant frequency as well as the cavity Q, providing more flexibility in the design.

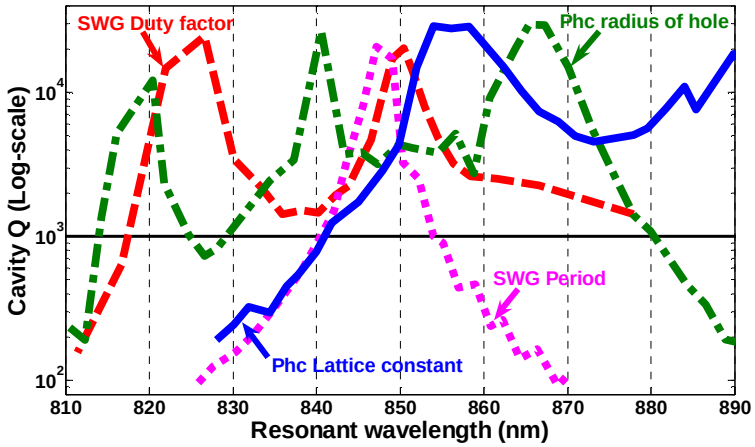

Fig. 10. Cavity Qs at resonances for the SWG and Phc VCSEL, lithographically (α , Λ , r, a) tuned.

5. Conclusion

We have presented a phase methodology to determine the phase of a single DBR, SWG, and Phc slab to be used as one of the mirrors in the VCSEL, and have estimated resonant wavelengths for the three different VCSEL structures. The maximum discrepancy between the FDTD phase and reflectance method was found to be less than 1.5nm throughout the simulations, indicating that our phase analysis is effective in accurately predicting resonances. The tunable range of the conventional VCSEL by adjustment of the cavity length was found to be about 76nm, compared to only 61nm and 48nm for SWG and Phc MEMS VCSEL.

Varying lithographically defined parameters, in particular, α (SWG) and r (Phc slab) allows for designing multi-wavelength arrays that can provide wide resonance tunability, which do not require a tuning voltage. We demonstrate that lithographical resonance tuning can be achieved up to a range of 60nm (SWG VCSEL) and 87nm (Phc VCSEL), while maintaining relatively high cavity Q values (>1,000). Phase and reflectivity peak are coincident for a broad range of FP wavelengths, resulting in a high cavity Q over a broad tuning range. This is a major improvement compared to the previous work in FP cavities in SWG [4]. Fabrications for the air-suspended SWGs and Phc slabs are currently in progress.

Acknowledgments

The authors would like to acknowledge the helpful advice and technical support of James Pond of Lumerical Solutions and our useful discussions with Behnam Faraji and Yiyi Zeng in Lukas Chrostowski's research group.

#82702 - $15.00 USD Received 3 May 2007; revised 3 Jul 2007; accepted 9 Jul 2007; published 1 Aug 2007